

12.1 A $210 \times 340 \times 50\mu\text{m}$ Integrated CMOS System for Micro-Robots with Energy Harvesting, Sensing, Processing, Communication and Actuation

Li Xu¹, Maya Lassiter², Xiao Wu¹, Yejoong Kim¹, Jungho Lee¹, Makoto Yasuda³, Masaru Kawaminami⁴, Marc Miskin², David Blaauw¹, Dennis Sylvester¹

¹University of Michigan, Ann Arbor, MI

²University of Pennsylvania, Philadelphia, PA

³United Semiconductor Japan, Kuwana, Japan

⁴United Semiconductor Japan, Yokohama, Japan

Built upon significant research into ultra-low power CMOS designs, complete sub-mm³ wireless sensor systems have been introduced [1-7] that include energy harvesting, sensing, processing, and communication. However, a key missing component in such systems is actuation, which could enable a host of new applications. Recently, a new class of electrochemical actuators that operate at low voltage and low power were developed [8]. The lithographic fabrication of these actuators is CMOS compatible, offering an unprecedented opportunity to create micron-scale, monolithic micro-robots. From a circuit point of view, such micro-robots face three design challenges: 1) energy harvesting and voltage generation in ultra-small form factor; 2) a customized processor for compute efficiency with stringent area budget; 3) an energy and area-efficient communication link.

To address these challenges, we present a $210\mu\text{m} \times 340\mu\text{m} \times 50\mu\text{m}$ CMOS die that integrates all the electronic functions necessary for a micro-robot, including bidirectional communication, sensing, processing, energy harvesting, and actuation. We also demonstrate integration of our circuits with electrochemical actuators and show leg movement when activated by a 60k lux light source. The proposed CMOS design employs p-n junctions to create two opposite-polarity solar cells and generate $> 0.6\text{V}$ to power the circuits and legs. The design implements ultra-low power ring-oscillator-based temperature sensors and electric field sensors (for neighbor proximity detection) to allow the robot to respond to external stimuli. An optical receiver (RX) is designed based on the architecture in [9] and uses an integrated CMOS solar cell as a light-sensing element. A custom processor with 11-bit instructions and high-level robot specific functions minimizes code size and power consumption. Each die is pre-assigned one of ten IDs, which are used as an address by the RX, allowing units in a robot swarm to be programmed with different programs and enabling robot collaboration. Uplink uses a visual cue approach (leg-waving), which maintains monolithic integration and low-power, in contrast to the use of stacked micro-LEDs [4,6] or a higher-power backscatter-based data uplink [7]. Finally, prior micro-systems typically use older technologies (e.g. 180nm [4]) that offer ultra-low leakage power but could not meet the logic area constraint for our micro-robot. Instead, we use a customized 55nm process with increased V_{th} 's that meets both the stringent leakage and area objectives.

Figure 12.1.1 shows the robot in [8] with electrochemical actuators and two fabricated p-n junctions, next to a biological microorganism (paramecium). The curvatures of these actuators change when they are biased relative to the surrounding aqueous electrolyte [8]. This robot, however, is passive, requiring laser light to be alternately directed to the front/rear p-n junctions to actuate the legs and induce motion. In contrast, the proposed micro-robot chip introduces intelligence and autonomous operations under constant ambient light to enable future deployment of swarms of robots (Fig. 12.1.1, bot, right). A group of these robots can potentially complete complex tasks at a microscopic level, such as monitoring cellular temperature and searching for living cells with abnormal metabolism [6] or assembling chipleths (microscale electronic modules) into circuits [10] (Fig. 12.1.1, bot, right).

The floorplan of the CMOS die includes four pads with top metal exposed to provide electrical connection to legs (Fig. 12.1.2). The active circuits are in the middle of the CMOS die, including temperature and electric field sensors on both sides, and are covered with customized metal structures and MIM capacitors to reduce the light-induced current by $\sim 10\times$, mitigating leakage power and timing errors. An array of unit solar cells occupy the top and bottom of the floorplan. The system clock is either generated on-chip with a leakage-based oscillator or recovered by the RX and locked to a transmitted optical clock (Fig. 12.1.2, top, right).

The entire system is fully powered by ambient light of as low as 60k lux. If the ambient light is weak, the system remains in *hibernation* or reset mode (Fig. 12.1.2, bot, right). Once sufficient light is received the *power-on* circuit wakes the robot and it executes a default program. The optical receiver is always on and continually monitors incoming light to detect whether a passcode is sent via modulated light. If a passcode is detected that matches the hardwired ID (which is also included in the top metal pattern for visual identification, Fig. 12.1.2) the robot changes to *attention* mode and receives instructions or a program. An error check is used to ensure correctness, after which the robot starts operating based on the received code.

To generate power for the whole system, including sufficient voltage for leg actuation, we must make full use of all possible p-n junctions due to the limited die area. As seen in Fig. 12.1.3, a triple-well CMOS process includes p-n diodes at N+ to P-well, P-well to deep-N-well, and deep-N-well to P-sub junctions. By connecting P-well to P-sub and N+ to deep-N-well, a *negative* solar cell unit is formed (Fig. 12.1.3, top, mid). A *positive* solar cell unit has similar connections but shorts P-sub to deep-N-well instead (Fig. 12.1.3, top, left). A pair of legs require a peak-to-peak voltage swing $> 0.6\text{V}$ to actuate, while the open-circuit voltage (without load) of a CMOS p-n diode is $< 0.5\text{V}$, even under $> 100\text{k lux}$ light. However, given the triple-well process, we float P-sub and stack the positive and negative solar cells, generating $> 0.6\text{V}$ across V_{DD} and V_{SSN} (Fig. 12.1.3). For the circuits on the die, all PMOS devices are in N-wells that are connected to V_{DD} and all NMOS are in P-wells that are connected to V_{SSN} with their deep-N-wells isolated from P-sub by connecting them to V_{DD} . Figure 12.1.3 shows the measured $V_{DD} - V_{SSN}$ (no load) under different light intensities. Note that because the robot operates in a fully untethered way, there is no ground and P-sub is biased at $\sim V_{DD}/2$. To actuate the legs, $V_{DD} - V_{SSN}$ is applied between a pair of front and rear legs (Fig. 12.1.3, mid, right). This configuration generates $> 0.3\text{V}$ and $< -0.3\text{V}$ on each leg, relative to the solution potential, which is sufficient to achieve curvature. Leg actuation is controlled using counters triggered by *clk_system*, and the period, phase, and pulse width of the leg actuation signals are configured with a resolution of one *clk_system* period.

The proposed micro-robot is guided by a customized processor with 11-bit instructions (Fig. 12.1.4). The processor takes input data from the optical receiver as well as the temperature and electric-field sensors and generates the actuation signals of the four legs (which includes uplink communication through waving) as outputs. Configuration values for all modules, including the leg frequency and phase, are memory mapped, as shown in Fig. 12.1.4 (bot, left). Both the instruction and data memories are implemented with flip-flops, and their reset values set a default configuration. In addition to conventional instructions, the processor employs high-level instructions specific to the robot function that greatly reduce code size, including *move* (with the direction and number of steps determined by configuration values), *temperature sense*, *electrical sense*, and *wave*. As an example, Fig. 12.1.4 (bottom) shows the temperature sense "TS" instruction format. The program demonstrated in measurements has 22 instructions, including 18 conventional instructions. A general purpose 32-bit low power processor, such as an ARM Cortex-M0, would instead require 34 instructions of 32 bit each, or 4x the memory footprint.

The proposed CMOS micro-robot die was fabricated in 55nm triple-well DDC process provided by United Semiconductor Japan, occupying an area of $210\mu\text{m} \times 340\mu\text{m}$. To reduce robot weight the CMOS die was thinned to $50\mu\text{m}$. We worked with the foundry to fabricate transistors with higher V_{th} s, reducing leakage by $\sim 9\times$ compared to the standard option, and allowing both power and area constraints to be met. Figure 12.1.5 presents measured waveforms showing untethered programming and operation. The chip was fully powered by 60k lux ambient light, and two oscilloscope probes ($10\text{M}\Omega \parallel 12\text{pF}$) were connected solely to record the voltages between the front legs (V_{FL} , V_{FR}) and V_{SSN} . The waveforms show that the micro-robot initially enters a default mode while it continues to check whether a passcode is being sent. An extra light source was then used to transmit a program and the micro-robot is shown to switch to attention mode and receive the program when it matches its chip ID. The program activates the front-right leg to turn left, then activates legs to move forward 5 steps and takes a temperature measurement. If the temperature exceeds a pre-defined threshold, it will stop and wave its front-right leg to uplink the measured temperature code using Manchester encoding.

We also successfully deposited two legs on a test die with identical harvesting and drive circuits (Fig. 12.1.5, bot, left). When activated with light (60k lux), leg actuation was observed, demonstrating the ability of the proposed circuits to initiate actuation. Figure 12.1.6 summarizes the performance and features of the proposed micro-robot design and compares it to prior state-of-the-art ultra-small microsystems. The proposed design is the first sub-mm³ chip design that includes energy harvesting, sensing, processing, communication, and actuation [1-8]. Figure 12.1.7 shows the chip micrograph of an array of micro-robot designs and a zoom-in of an individual system.

References:

- [1] J. Lee et al., "Neural recording and stimulation using wireless networks of microimplants," *Nat. Electron.*, 4, 604-614 (2021).
- [2] C. Shi et al., "Application of a sub-0.1-mm³ implantable mote for in vivo real-time wireless temperature sensing," *Sci. Adv.* 2021, May 7, 7(19): eabf6312.
- [3] M. X. Yang et al., "Intracellular detection and communication of a wireless chip in cell," *Sci. Rep.*, 11, 5967 (2021).
- [4] J. Lim et al., "A Light Tolerant Neural Recording IC for Near-Infrared-Powered Free Floating Motes," *IEEE Symp. VLSI Circuits*, 2021.
- [5] Alejandro J. Cortese et al., "Microscopic sensors using optical wireless integrated circuits," *Proc. Nat. Academy of Sciences*, Apr 2020, 117 (17) 9173-9179.

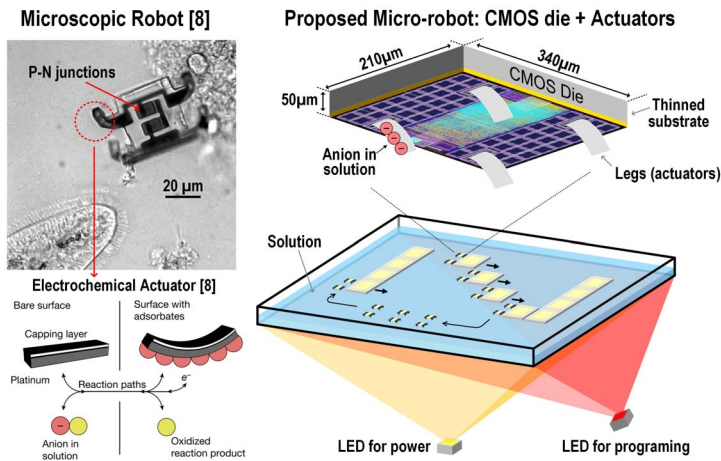


Figure 12.1.1: Proposed micro-robot that consists of a CMOS die and electrochemical actuators; vision of groups of micro-robots assembling chipllets.

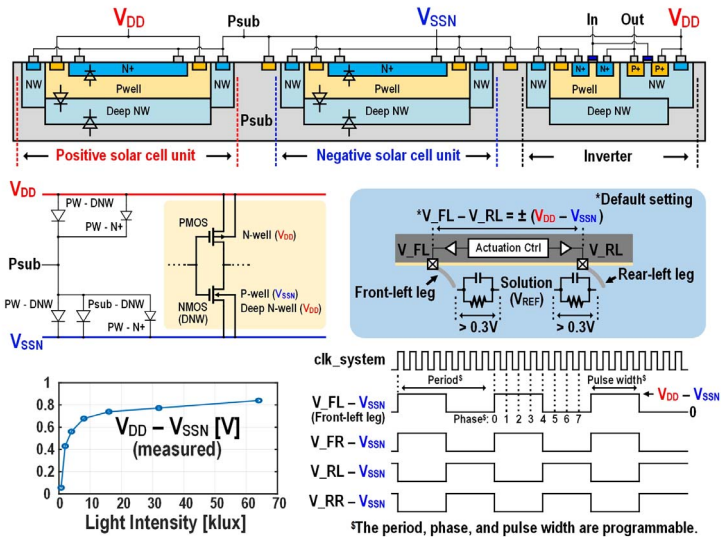


Figure 12.1.3: Cross section of the well structures for positive solar cell unit, negative solar cell unit, and an inverter in the proposed design; programmable leg actuation and voltage waveforms.

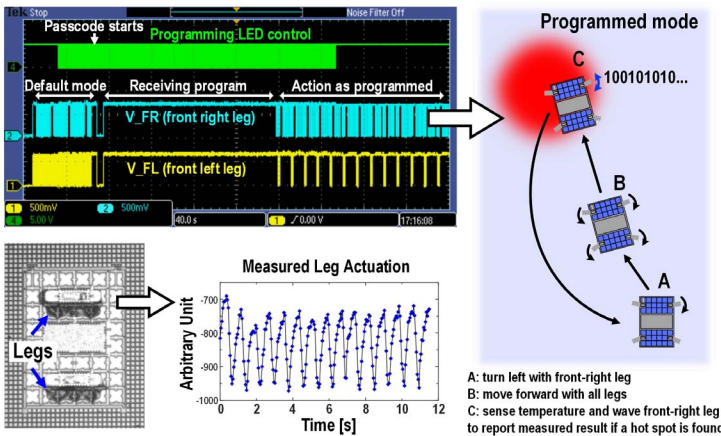


Figure 12.1.5: Measured waveforms of front-left and front-right legs during untethered programming; two legs deposited on a test die and measured curvature of the leg during untethered testing (fully powered by light).

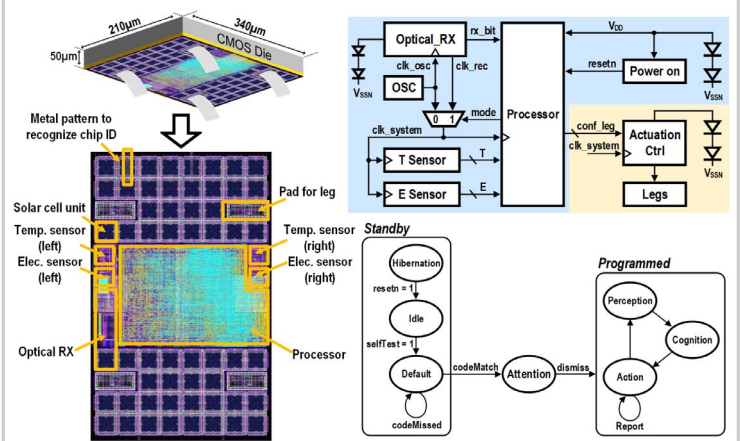


Figure 12.1.2: Layout and floorplan of the proposed CMOS system; high-level diagram of the proposed design; operation states of the proposed micro-robot that supports both default mode and untethered programming.

12

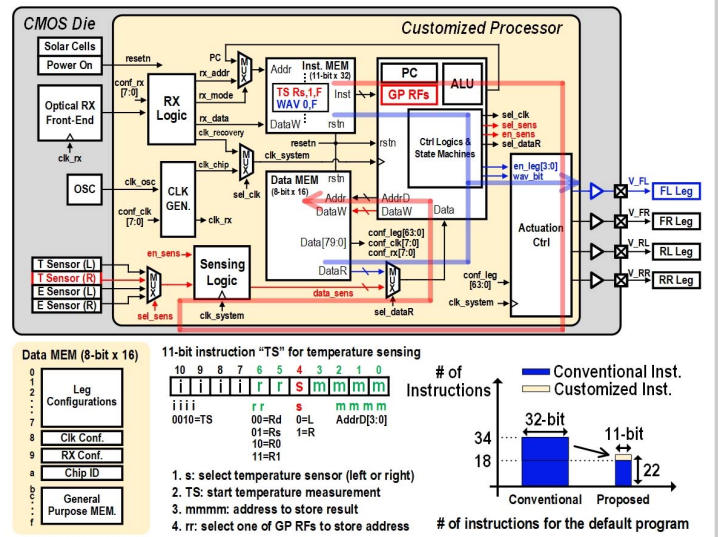


Figure 12.1.4: Customized processor in the proposed CMOS system; datapaths of two instructions ("TS Rs, 1, F" and "WAV 0, F") for temperature sensing and leg-waving (uplink); customized 11-bit instructions.

	This work	VLSI'2021 [4]	Nature'2020 [8]	PNAS'2020 [5]	VLSI'2018 [6]	RFIC'2017 [7]
Technology	55nm	180nm	n/a	n/a	55nm	65nm
Sensor	Temperature + Electric Field	Neural Recording	No	Voltage + Temperature + Pressure + Conductivity	Temperature	Glucose Concentration
System Dimension	210 x 340 x 50µm	190 x 280 x n/a µm	40 x 40 x 5µm	8 x 65 x 100µm	360 x 400 x 280µm	200 x 200 x 100µm
System Power	75nW*	570nW (38°C)	n/a	~10µW	16nW	63nW
Integrated Processor	Yes	No	No	No	Yes	No
Downlink	Optical	Optical	No	No	Optical	Optical
Uplink	Leg-waving	Micro-LED	No	Micro-LED	Micro-LED	Backscatter
Transmit Distance	Camera limited (>2cm as measured)	n/a	n/a	> 5mm	15.6cm	2mm
System Integration	Monolithic fabrication	Stack with flip chip	Monolithic fabrication	Monolithic fabrication	Stack with wire bonding	TSV to the back of die
Actuation	Electrochemical actuators	No	Electrochemical actuators	No	No	No
Robot?	Yes	No	No	No	No	No

*Without legs, measured system power is 15nW.

Figure 12.1.6: Comparison with the prior state-of-the-art microsystems.

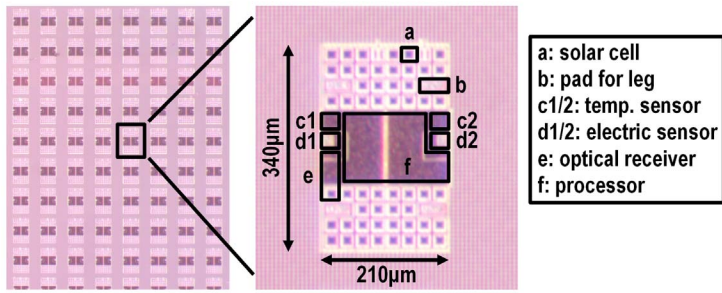


Figure 12.1.7: Chip micrograph of the micro-robot design array and zoom-in of an individual CMOS system.

Additional References:

- [6] X. Wu et al., "A 0.04mm³ 16nW Wireless and Batteryless Sensor System with Integrated Cortex-M0+ Processor and Optical Communication for Cellular Temperature Measurement," *IEEE Symp. VLSI Circuits*, Honolulu, 2018, pp. 191-192.
- [7] S. O'Driscoll et al., "A 200µm × 200µm × 100µm, 63nW, 2.4GHz injectable fully-monolithic wireless bio-sensing system," *IEEE RFIC Symposium*, Honolulu, 2017, pp. 256-259.
- [8] M.Z. Miskin, A.J. Cortese, K. Dorsey et al., "Electronically integrated, mass-manufactured, microscopic robots," *Nature* 584, 557-561 (2020).
- [9] W. Lim, T. Jang, I. Lee et al., "A 380pW dual mode optical wake-up receiver with ambient noise cancellation," *IEEE Symp. VLSI Circuits*, 2016.
- [10] T. Simonite, "To keep pace with Moore's law, chipmakers turn to chiplets," *Wired Magazine*, 15(6):533-556, November 2018.